Journal of Sound and Vibration 329 (2010) 893–911

Contents lists available at ScienceDirect

Journal of Sound and Vibration

journal homepage: www.elsevier.com/locate/jsvi

Modal analysis of a continuous gyroscopic second-order system with nonlinear constraints

M.R. Brake [a,*], J.A. Wickert [b]

[a] Applied Mechanics Development Department, Sandia National Laboratories, Albuquerque, NM 87185, USA[1]
[b] Department of Mechanical Engineering, Iowa State University, Ames, IA 50011, USA

ARTICLE INFO

Article history:
Received 10 April 2009
Received in revised form
1 October 2009
Accepted 2 October 2009
Handling Editor: L.N. Virgin
Available online 24 October 2009

ABSTRACT

A method for the modal analysis of continuous gyroscopic systems with nonlinear constraints is developed. This method assumes that the nonlinear constraint can be expressed as a piecewise linear force–deflection profile located at an arbitrary position within the domain. Using this assumption, the mode shapes and natural frequencies are first found for each state, then a mapping method based on the inner product of the mode shapes is developed to map the displacement of the system between the in-contact and out-of-contact states. To illustrate this method, a model for the vibration of a traveling string in contact with a piecewise-linear constraint is developed as an analog of the interaction between magnetic tape and a guide in data storage systems. Five design parameters of the guide are considered: flange clearance, flange stiffness, symmetry of the force–deflection profile in terms of flange stiffness and offset, and the guide's position along the length of the string. There are critical bifurcation thresholds, below which the system exhibits no chaotic behavior and is dominated by period one, symmetric behavior, and above which the system contains asymmetric, higher periodic motion with windows of chaotic behavior. These bifurcation thresholds are particularly pronounced for the transport speed, flange clearance, symmetry of the force deflection profile, and guide position. The stability of the system is sensitive to the system's velocity, and, compared to stationary systems, more mode shapes are needed to accurately model the dynamics of the system.

Published by Elsevier Ltd.

1. Introduction

Gyroscopic systems are classified as systems that vibrate about a state of mean rotation or translation, and the Lagrangian of these systems contains terms that are linear in the generalized velocities. Linear and nonlinear constraints in gyroscopic systems include transverse cracks in rotating shafts [1], clearances of fluid conveying pipes [2], and axially moving webs that have rigid or compliant guides [3]. In the absence of these constraints, exact, closed form solutions for the vibration of gyroscopic systems are available through Laplace transform methods [4] and modal analysis and Green's function methods [5]. Similar solution methods are developed for gyroscopic systems with linear constraints by dividing the system into two contiguous regions divided at the point of the linear constraint [6–8].

* Corresponding author.
E-mail address: mrbrake@sandia.gov (M.R. Brake).

[1] Sandia National Laboratories is a multiprogram laboratory operated by Sandia Corporation, a Lockheed Martin Company, for the United States Department of Energy's National Nuclear Security Administration under Contract DE-AC04-94-AL85000.

0022-460X/$ - see front matter Published by Elsevier Ltd.
doi:10.1016/j.jsv.2009.10.004

Piecewise-linear and nonlinear non-gyroscopic systems are typically analyzed using a Poincaré mapping method where the state of the system before contact is mapped to the state of the system after contact [9–11]. Similarly, an algebraic mapping method can be used for continuous systems with an amplitude constraint modeled as a piecewise-linear spring [12], with the solution between state changes found via modal analysis [12,13]. Nonlinear systems with a sufficiently large parameter space may be designed to eliminate certain instabilities, such as jump phenomena in the bifurcation diagrams [14,15].

Gyroscopic systems have higher characteristic bifurcation thresholds, and thus larger stable regimes, than non-gyroscopic systems [1]. The stability of gyroscopic systems is further influenced by the stiffness of the nonlinearity: in systems with very stiff constraints, the range of period doubling bifurcations is significantly smaller than in systems with less stiff constraints [16]. Existing solutions for gyroscopic systems with nonlinear constraints do not include exact, closed form or asymptotic approximation approaches such as modal analysis, and instead rely on time-consuming numerical methods. Below the characteristic bifurcation threshold, analytical estimates of the nonlinear modes' periods are available through a complex normal mode approach [1], and for systems with cubic nonlinearities, solutions are obtainable by a differential quadrature method [17,18].

In the present study, a model is developed for a traveling string in contact with a piecewise-linear guide in Section 2 as an analog to the dynamics of magnetic tape in contact with a nonlinear guide in order to illustrate the proposed solution method. The vibration of magnetic tape is an application related to the broader problem area encompassing the mechanics of axially moving materials [19] and web transport systems [20,21]. Vibration models that are typically applied to represent magnetic tape include traveling strings [22] and traveling tensioned beams [23]. The displacement of the string is solved via modal analysis in Section 2.1, and in Section 2.2 a mapping method is developed to map the state of the system across contact with the guide's flanges. In Section 3, parameter studies are conducted on the guide's stiffness, clearance, symmetry, and position. The response of the system shows that critical bifurcation thresholds exist, above which the system exhibits asymmetric motion, bifurcations, and chaotic behavior.

2. Vibration model

In the system of Fig. 1(a), a string of length L, tension P, and mass per unit of length ρ travels between two pinned guides with transport speed V. At the string's left boundary ($X=0$), the pinned guide has prescribed lateral displacement $W(0,T)=A\sin(\Omega T)$ at time T with excitation frequency Ω. A nonlinear guide is located at $X=L_1$, and the displacement $W(X,T)$ of the string is divided into three states: the string is in contact with the lower flange of the guide $j=-1$, the string is not in contact with either flange $j=0$, and the string is in contact with the top flange $j=1$. The guide has arbitrary

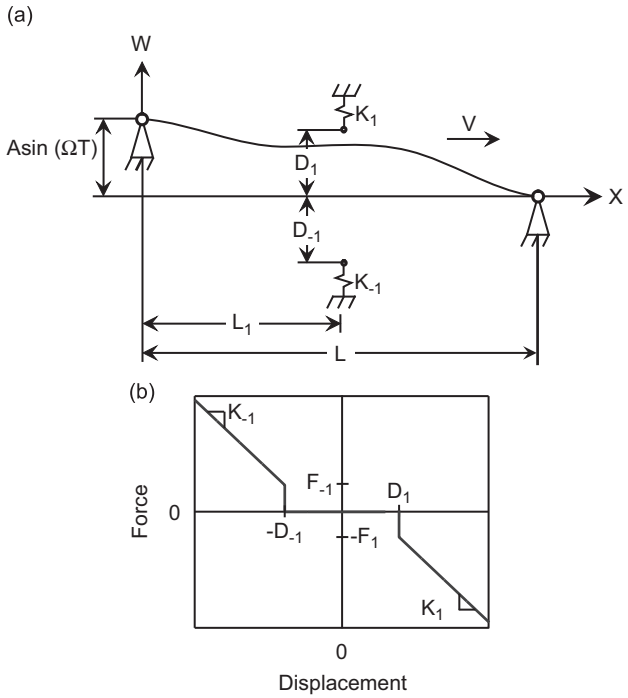

Fig. 1. (a) Schematic of the system with boundary excitation and a nonlinear guide located at $X=L_1$ with (b) an arbitrary force–deflection constitutive relationship.

clearance D_j, stiffness K_j, and preload F_j

$$D_j = \begin{cases} D_1 & : j = 1 \\ 0 & : j = 0 \\ -D_{-1} & : j = -1 \end{cases} \quad K_j = \begin{cases} K_1 & : j = 1 \\ 0 & : j = 0 \\ K_{-1} & : j = -1 \end{cases} \quad F_j = \begin{cases} -F_1 & : j = 1 \\ 0 & : j = 0 \\ F_{-1} & : j = -1, \end{cases} \tag{1}$$

illustratively shown in Fig. 1(b). By defining the dimensionless quantities

$$v = V\sqrt{\frac{\rho}{P}}, \quad t = T\sqrt{\frac{P}{\rho L^2}}, \quad \omega = \Omega\sqrt{\frac{\rho L^2}{P}}, \quad k_j = \frac{K_j L}{P}, \quad f_j = \frac{F_j}{P},$$

$$a = \frac{A}{L}, \quad \ell_1 = \frac{L_1}{L}, \quad w = \frac{W}{L}, \quad x = \frac{X}{L}, \quad d_j = \frac{D_j}{L}, \tag{2}$$

the non-dimensional equation of motion in the j th state is [5]

$$w_{,tt} + 2vw_{,xt} + (v^2 - 1)w_{,xx} + k_j w\delta(x - \ell_1) = (f_j + k_j d_j)\delta(x - \ell_1), \tag{3}$$

where δ denotes the Dirac delta function, with boundary and initial conditions

$$w(0,t) = a\sin(\omega t), \quad w(1,t) = 0, \tag{4}$$

$$w(x,0) = z_0(x), \quad w_{,x}(x,0) = s_0(x), \tag{5}$$

and a comma subscript denotes partial differentiation.

2.1. Modal analysis

The general solution method is to consider the modal analysis of the various states of the system separately, and then to develop a state-to-state mapping based on the orthogonality of the mode shapes. For the present system, two cases are considered in the modal analysis: the string is not in contact with either flange $j = 0$ and has displacement w_0, and the string is in contact with either the top or bottom flange $j \neq 0$. The modal coordinates are of a piecewise nature, with separate solutions when the string is in contact with either flange and when the string is out of contact with both flanges. When the string is in contact with either flange, it is conceptually divided into two contiguous regions $R_1 = x \in (0, \ell_1)$ and $R_2 = x \in (\ell_1, 1)$ with displacement w_1 over R_1 and w_2 over R_2. Taking a control volume about $x = \ell_1$, a force balance yields

$$(1 - v^2)(w_{2,x}(\ell_1,t) - w_{1,x}(\ell_1,t)) - k_j(w_1(\ell_1,t) - d_j) + f_j = 0, \tag{6}$$

and continuity requires

$$w_2(\ell_1,t) - w_1(\ell_1,t) = 0. \tag{7}$$

Defining the equivalent offset of the spring due to the preload

$$y_j = \begin{cases} -f_1/k_1 & : j = 1 \\ 0 & : j = 0 \\ f_{-1}/k_{-1} & : j = -1, \end{cases} \tag{8}$$

and matching the displacement at the boundaries and the difference between d_j and y_j at $x = \ell_1$, the superposition that results in homogeneous boundary conditions is found as

$$w_m(x,t) = u_m(x,t) + \left(a\sin(\omega t) + \left(\frac{d_j - y_j}{\ell_1(1-\ell_1)} - \frac{|j| + \ell_1}{\ell_1}a\sin(\omega t)\right)x + \left(-\frac{d_j - y_j}{\ell_1(1-\ell_1)} + \frac{|j|}{\ell_1}a\sin(\omega t)\right)x^2\right), \tag{9}$$

with $m = 0, 1, 2$. The equation of motion becomes

$$u_{m,tt} + 2vu_{m,xt} + (v^2 - 1)u_{m,xx} = f_{sj}, \tag{10}$$

with boundary conditions

$$u_0(0,t) = 0, \quad u_0(1,t) = 0, \tag{11}$$

$$u_1(0,t) = 0,$$

$$u_2(\ell_1,t) - u_1(\ell_1,t) = 0,$$

$$(1 - v^2)(u_{2,x}(\ell_1,t) - u_{1,x}(\ell_1,t)) - k_j u_1(\ell_1,t) = 0,$$

$$u_2(1,t) = 0, \tag{12}$$

and forcing function

$$f_{sj} = \left(|j|\frac{\omega^2}{\ell_1}x^2 - \omega^2\frac{|j|+\ell_1}{\ell_1}x + \left(\omega^2 - \frac{2|j|}{\ell_1}(\nu^2-1)\right)\right)a\sin(\omega t) - 2\nu a\omega\left(\frac{2|j|}{\ell_1}x - \frac{|j|+\ell_1}{\ell_1}\right)\cos(\omega t) + 2(\nu^2-1)\frac{d_j - y_j}{\ell_1(1-\ell_1)}. \tag{13}$$

Assuming the separable solution

$$u_m(x,t) = \mathrm{e}^{\mathrm{i}\omega_{jn}t}\phi_{jmn}(x), \tag{14}$$

where $\mathrm{i} = \sqrt{-1}$ and ω_{jn} is the n th natural frequency in state j with corresponding mode shape ϕ_{jmn}, the eigenvalue problem

$$\begin{gathered}(\nu^2-1)\phi''_{jmn} + \mathrm{i}2\nu\omega_{jn}\phi'_{jmn} - \omega_{jn}^2\phi_{jmn} = 0,\\ \phi_{00n}(0) = 0, \quad \phi_{j1n}(0) = 0,\\ \phi_{j1n}(\ell_1) - \phi_{j2n}(\ell_1) = 0,\\ (1-\nu^2)(\phi_{j2n}'(\ell_1) - \phi_{j1n}'(\ell_1)) - k_j\phi_{j1n}(\ell_1) = 0,\\ \phi_{00n}(1) = 0, \quad \phi_{j2n}(1) = 0\end{gathered} \tag{15}$$

has solution

$$\phi_{jmn} = \alpha_1\mathrm{e}^{\gamma_1 x} + \alpha_2\mathrm{e}^{\gamma_2 x}, \tag{16}$$

which leads to the dispersion relation

$$\begin{gathered}\gamma^2 + \frac{\mathrm{i}2\nu\omega_{jmn}}{\nu^2-1}\gamma - \frac{\omega_{jmn}^2}{\nu^2-1} = 0,\\ \gamma_{1,2} = \mathrm{i}\frac{\omega_{jmn}}{1-\nu^2}(\nu\pm 1).\end{gathered} \tag{17}$$

Application of the boundary conditions for $j = 0$ yields the natural frequencies for vibration out of contact with the flanges

$$\omega_{0n} = n\pi(1-\nu^2), \tag{18}$$

and the mode shapes

$$\phi_{00n}(x) = \alpha_{0n}\mathrm{e}^{\mathrm{i}n\pi\nu x}\sin(n\pi x) \tag{19}$$

are the eigenfunctions of the classical moving string [5]. It follows from applying the boundary conditions for the in-contact system that the mode shapes in state j for the first ϕ_{j1n} and second ϕ_{j2n} spans are

$$\begin{gathered}\phi_{j1n} = \alpha_{jn}\mathrm{e}^{\mathrm{i}\nu\omega_{jn}/(1-\nu^2)}\sin\left(\frac{\omega_{jn}}{1-\nu^2}x\right),\\ \phi_{j2n} = \alpha_{jn}\mathrm{e}^{\mathrm{i}\nu\omega_{jn}/(1-\nu^2)}\left(\sin\left(\frac{\omega_{jn}}{1-\nu^2}x\right) - \tan\left(\frac{\omega_{jn}}{1-\nu^2}\right)\cos\left(\frac{\omega_{jn}}{1-\nu^2}x\right)\right).\end{gathered} \tag{20}$$

To compactly represent the in-contact mode shapes and displacements ($j \neq 0$)

$$\phi_{jn} = \begin{cases}\phi_{j1n} : x \in R_1\\ \phi_{j2n} : x \in R_2\end{cases} \quad u_j = \begin{cases}u_1 : x \in R_1\\ u_2 : x \in R_2.\end{cases}$$

Similarly, the out-of-contact mode shapes are rewritten as $\phi_{0n} = \phi_{00n}$. Application of the boundary conditions yields the equation for the natural frequencies when the string is in contact with the guide [6]

$$k_j\sin\left(\frac{\omega_{jn}(1-\ell_1)}{1-\nu^2}\right)\sin\left(\frac{\omega_{jn}\ell_1}{1-\nu^2}\right) + \omega_{jn}\sin\left(\frac{\omega_{jn}}{1-\nu^2}\right) = 0. \tag{21}$$

Defining the mass, gyroscopic, and stiffness operators that act over $x \in [R_1, R_2]$

$$\begin{gathered}\mathrm{M} = I\bullet,\\ \mathrm{G} = 2\nu\frac{\partial}{\partial x}\bullet,\\ \mathrm{K}_j = (\nu^2-1)\frac{\partial^2}{\partial x^2}\bullet,\end{gathered} \tag{22}$$

the equation of motion is cast in matrix operator form [5]

$$\mathbf{A}_j\mathbf{u}_{j,t} + \mathbf{B}_j\mathbf{u}_j = \mathbf{q}_j,$$

$$\mathbf{A}_j = \begin{bmatrix} \mathrm{M} & 0 \\ 0 & \mathrm{K}_j \end{bmatrix}, \quad \mathbf{B}_j = \begin{bmatrix} \mathrm{G} & \mathrm{K}_j \\ -\mathrm{K}_j & 0 \end{bmatrix},$$

$$\mathbf{u}_j = \begin{Bmatrix} u_{j,t} \\ u_j \end{Bmatrix}, \quad \mathbf{q}_j = \begin{Bmatrix} f_{sj} \\ 0 \end{Bmatrix} \tag{23}$$

with mode shapes

$$\boldsymbol{\psi}_{jn} = \begin{Bmatrix} \lambda_{jn}\phi_{jn} \\ \phi_{jn} \end{Bmatrix} \tag{24}$$

and response

$$\mathbf{u}_j = \sum_{n=\pm1,\pm2,\ldots}^{\pm N} \eta_{jn}(t)\boldsymbol{\psi}_{jn}(x), \tag{25}$$

where N is the number of mode shapes taken and η_{jn} are the modal coefficients for the n th mode of the j th state. Modal damping is introduced following the procedure of [24] by using $\lambda_{jn} = \omega_{jn}(-\zeta + \mathrm{i})$, where ζ is the modal damping coefficient. In order to represent the response in a compact manner [25]

$$\lambda_{j-n} = \overline{\lambda_{jn}}, \quad \boldsymbol{\psi}_{j-n} = \overline{\boldsymbol{\psi}_{jn}} \tag{26}$$

for $n = 1, 2, \ldots, N$, with the complex conjugate denoted by an over-bar. Defining the inner product for two arbitrary vectors $\mathbf{b}_1$ and $\mathbf{b}_2$ as

$$\langle \mathbf{b}_1, \mathbf{b}_2 \rangle = \int_0^1 \mathbf{b}_1^{\mathrm{T}}\overline{\mathbf{b}_2}\,\mathrm{d}x, \tag{27}$$

the mode shapes are normalized with respect to $\mathbf{A}_j$ such that

$$\langle \mathbf{A}_j\boldsymbol{\psi}_{jn}, \boldsymbol{\psi}_{jm} \rangle = \delta(n-m) \tag{28}$$

for $n, m = \pm1, \pm2, \ldots, \pm N$. Using the superposition (9), the initial conditions (5) become

$$\mathbf{u}_{j0}(x,t_0) = \begin{Bmatrix} z_0 - a\sin(\omega t_0)\left(\dfrac{|j|}{\ell_1}x^2 - \dfrac{|j|+\ell_1}{\ell_1}x + 1\right) + \dfrac{d_j - y_j}{\ell_1(1-\ell_1)}(x^2-1) \\ s_0 - a\omega\cos(\omega t_0)\left(\dfrac{|j|}{\ell_1}x^2 - \dfrac{|j|+\ell_1}{\ell_1}x + 1\right) \end{Bmatrix}, \tag{29}$$

and the modal coefficients are calculated through

$$\eta_{jn}(t) = \hat{\eta}_{jn}\mathrm{e}^{\lambda_{jn}(t-t_0)} + \int_{t_0}^{t} \mathrm{e}^{\lambda_{jn}(t-\tau)}q_{jn}(\tau)\,\mathrm{d}\tau, \tag{30}$$

$$\hat{\eta}_{jn} = \int_0^1 \{\mathbf{A}_j\mathbf{u}_{j0}\}^{\mathrm{T}}\overline{\boldsymbol{\psi}}_{jn}\,\mathrm{d}x, \tag{31}$$

$$q_{jn}(t) = \int_0^1 \mathbf{q}_j^{\mathrm{T}}\overline{\boldsymbol{\psi}}_{jn}\,\mathrm{d}x. \tag{32}$$

2.2. State-to-state mapping

Mappings between the modal coordinates are needed for each set of states in the system. In the present system, there are three different state-to-state mappings: from no contact to flange contact ($j = 0$ to ±1), from flange contact to no contact ($j = \pm1$ to 0), and from contact with one flange to contact with the other flange ($j = \pm1$ to ∓1, $d_{-1} = d_1 = 0$). The string vibrates in the $j = 0$ state until it contacts the flange associated with state j

$$u_0(\ell_1, t) = d_j - a\sin(\omega t)(1-\ell_1), \tag{33}$$

which corresponds to the gap between the string and the flange vanishing. The string continues to vibrates in state $j \neq 0$ until it loses contact

$$u_j(\ell_1, t) = y_j. \tag{34}$$

By contrast with the transition to contact, the transition out of contact can be determined by calculating the time at which the normal force between the string and the flange vanishes.

For $t_0>0$, the initial conditions z_0 and s_0 (29) are expressed in terms of the mode shapes and superpositions from the previous state. Defining i as the previous state, the state-to-state mapping follows from the orthogonality of the mode shapes

$$\hat{\boldsymbol{\eta}}_j = \mathbf{T}^{i,j}\boldsymbol{\eta}_i(t_0) + \Gamma_1^{i,j}(t_0)\mathbf{g}_1^j + \Gamma_2^{i,j}(t_0)\mathbf{g}_2^j + \Gamma_3^{i,j}(t_0)\mathbf{g}_3^j, \tag{35}$$

$$\hat{\boldsymbol{\eta}}_j = \begin{Bmatrix} \hat{\eta}_{j1} \\ \hat{\eta}_{j-1} \\ \hat{\eta}_{j2} \\ \vdots \\ \hat{\eta}_{j-N} \end{Bmatrix}, \quad \boldsymbol{\eta}_j(t) = \begin{Bmatrix} \eta_{j1}(t) \\ \eta_{j-1}(t) \\ \eta_{j2}(t) \\ \vdots \\ \eta_{j-N}(t) \end{Bmatrix}, \tag{36}$$

with constant terms

$$\mathbf{T}^{i,j} = \begin{bmatrix} \langle \mathbf{A}_j\boldsymbol{\psi}_{i1}, \boldsymbol{\psi}_{j1} \rangle & & \cdots & & \langle \mathbf{A}_j\boldsymbol{\psi}_{i-N}, \boldsymbol{\psi}_{j1} \rangle \\ & \ddots & & & \\ \vdots & & \langle \mathbf{A}_j\boldsymbol{\psi}_{im}, \boldsymbol{\psi}_{jn} \rangle & & \vdots \\ & & & \ddots & \\ \langle \mathbf{A}_j\boldsymbol{\psi}_{i1}, \boldsymbol{\psi}_{j-N} \rangle & & \cdots & & \langle \mathbf{A}_j\boldsymbol{\psi}_{i-N}, \boldsymbol{\psi}_{j-N} \rangle \end{bmatrix}, \tag{37}$$

$$\mathbf{g}_1^j = \begin{Bmatrix} \int_0^1 \overline{\phi_{j1}}\,\mathrm{d}x \\ \int_0^1 \overline{\phi_{j-1}}\,\mathrm{d}x \\ \int_0^1 \overline{\phi_{j2}}\,\mathrm{d}x \\ \vdots \\ \int_0^1 \overline{\phi_{j-N}}\,\mathrm{d}x \end{Bmatrix}, \tag{38}$$

$$\mathbf{g}_2^j = \begin{Bmatrix} \int_0^1 \frac{1}{\ell_1}(x^2-x)\overline{\lambda_{j1}\phi_{j1}}\,\mathrm{d}x \\ \int_0^1 \frac{1}{\ell_1}(x^2-x)\overline{\lambda_{j-1}\phi_{j-1}}\,\mathrm{d}x \\ \int_0^1 \frac{1}{\ell_1}(x^2-x)\overline{\lambda_{j2}\phi_{j2}}\,\mathrm{d}x \\ \vdots \\ \int_0^1 \frac{1}{\ell_1}(x^2-x)\overline{\lambda_{j-N}\phi_{j-N}}\,\mathrm{d}x \end{Bmatrix}, \tag{39}$$

$$\mathbf{g}_3^j \begin{Bmatrix} \overline{\phi_{j1}(\ell_1)} \\ \overline{\phi_{j-1}(\ell_1)} \\ \overline{\phi_{j2}(\ell_1)} \\ \vdots \\ \overline{\phi_{j-N}(\ell_1)} \end{Bmatrix}, \tag{40}$$

and time dependent terms

$$\Gamma_1^{i,j}(t_0) = \begin{cases} \left(a\sin(\omega t_0) - \dfrac{d_i - y_i}{1-\ell_1}\right)\dfrac{2}{\ell_1}(\nu^2-1) & : j = 0 \\ \left(\dfrac{d_j - y_j}{1-\ell_1} - a\sin(\omega t_0)\right)\dfrac{2}{\ell_1}(\nu^2-1) & : i = 0 \text{ and } j \neq 0 \\ -2\dfrac{y_j - y_i}{\ell_1(1-\ell_1)}(\nu^2-1) & : i \neq 0 \text{ and } j \neq 0, \end{cases} \tag{41}$$

$$\Gamma_2^{i,j}(t_0) = \begin{cases} a\omega\cos(\omega t_0) & : j = 0 \\ -a\omega\cos(\omega t_0) & : i = 0 \text{ and } j \neq 0 \\ 0 & : i \neq 0 \text{ and } j \neq 0, \end{cases} \tag{42}$$

$$\Gamma_3^{i,j}(t_0) = \begin{cases} 0 & : j = 0 \\ k_j(a\sin(\omega t_0)(1-\ell_1) - (d_j - y_j)) & : i = 0 \quad \text{and} \quad j \neq 0 \\ k_j(y_j - y_i) & : i \neq 0 \quad \text{and} \quad j \neq 0. \end{cases} \tag{43}$$

The mapping (35) transforms the previous set of modal coordinates $\boldsymbol{\eta}_i(t)$ in state i at the transition time t_0 to the initial modal coordinates $\hat{\boldsymbol{\eta}}_j$ in the new state taking into consideration the change in the superposition function. The mapping consists of constant matrices $\mathbf{T}^{i,j}$ that are based on the inner products of the mode shapes, and constant vectors $\mathbf{g}_1^j$, $\mathbf{g}_2^j$, and $\mathbf{g}_3^j$ and time dependent coefficients $\Gamma_1^{i,j}(t_0)$, $\Gamma_2^{i,j}(t_0)$, and $\Gamma_3^{i,j}(t_0)$ that are based on the superposition functions. In the symmetric case, $\mathbf{T}^{i,j}$ reduces to the identity matrix for $i,j \neq 0$. In simulation, the constant matrices and vectors (37)–(40) are calculated once and the displacement between state changes is given in an asymptotic expansion from the modal analysis. At the instant that a flange is engaged or disengaged, the time dependent terms (41)–(43) are calculated and Eq. (35) maps the modal coordinates from the previous state to the next state.

Table 1
Baseline parameters for the system of Fig. 1(a).

Variable	Baseline value
Excitation amplitude, a	7.7×10^{-4}
Clearance of the lower flange, d_{-1}	1.9×10^{-4}
Clearance of the upper flange, d_1	1.9×10^{-4}
Preload of the lower flange, f_{-1}	0
Preload of the upper flange, f_1	0
Stiffness of the lower flange, k_{-1}	30
Stiffness of the upper flange, k_1	30
Position of the guide, ℓ_1	0.5
Number of modes, N	10
Transport speed, v	0.068
Modal damping coefficient, ζ	0.04

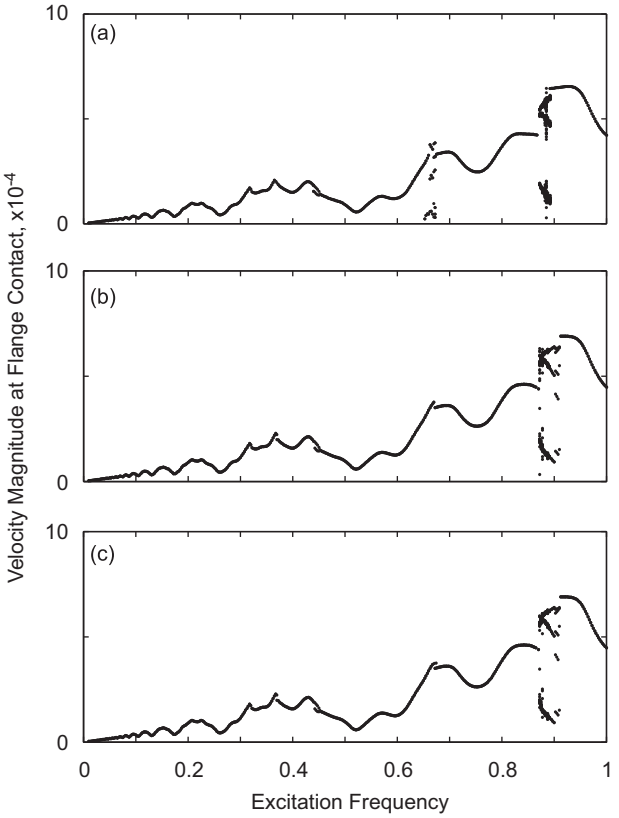

Fig. 2. Convergence of the frequency response for (a) $N = 5$, (b) $N = 10$, and (c) $N = 100$.

3. Frequency response

The frequency response function is taken as the magnitude of the velocity of the string at $x = \ell_1$ when it impacts a flange. The stable response is calculated after the vibration has reached a steady-state. While this method is well suited to finding the stable branches of the response, another approach, such as an asymptotic method [26], is needed to capture the unstable branches of the response. The properties of the string and guide are representative of magnetic tape systems and are listed in Table 1. While the nonlinear guide located at the midspan in the system of Fig. 1(a) is symmetric in terms of the physical layout, the response at certain frequencies is asymmetric (meaning that the magnitude of impact against the upper and lower flanges is different), similar to other piecewise-linear systems with deadbands in displacement [27]. There are often multiple coexisting stable solutions, which can be found via appropriate initial conditions. The two stable responses occur simultaneously, one on contact with the upper flange and the other on contact with the lower flange. Proper selection of the initial conditions determines which solution will occur on a flange. In the following parameter studies, all stable solutions of the frequency response are plotted together. The response of the system described by the

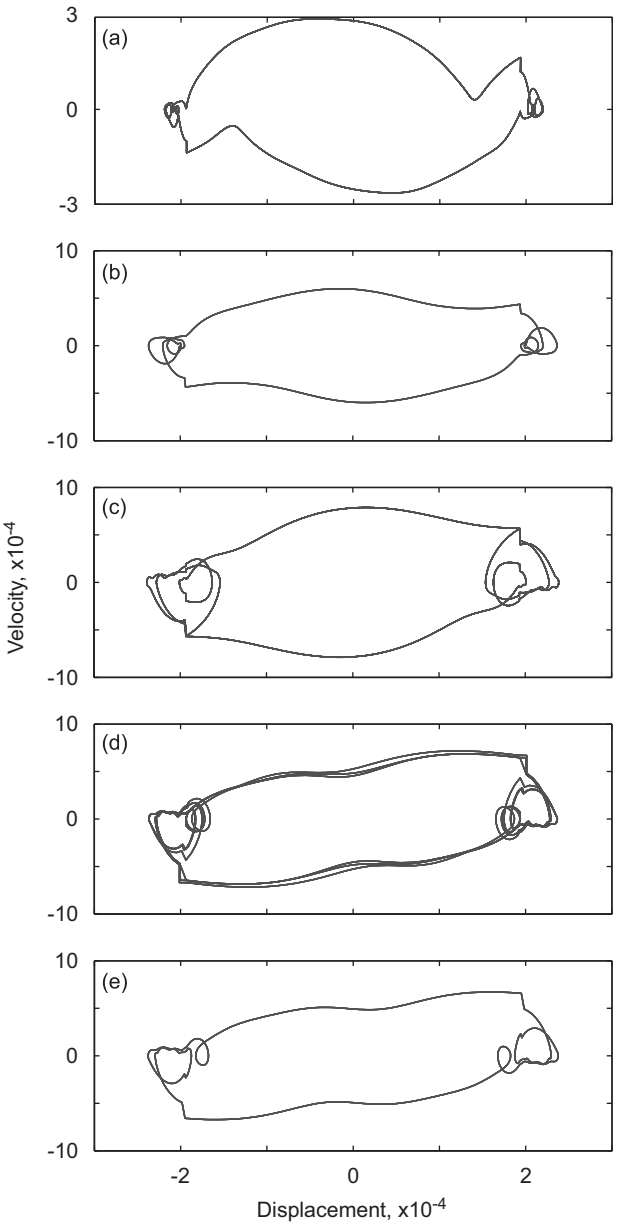

Fig. 3. Phase projections for the parameters of Table 1 showing (a) asymmetric 1–1 motion ($\omega = 0.445$), (b) symmetric 1–1 motion ($\omega = 0.87245$), (c) symmetric 1–3 motion ($\omega = 0.87248$), (d) symmetric 3–2 motion ($\omega = 0.924$), and (e) symmetric 1–2 motion ($\omega = 0.94$).

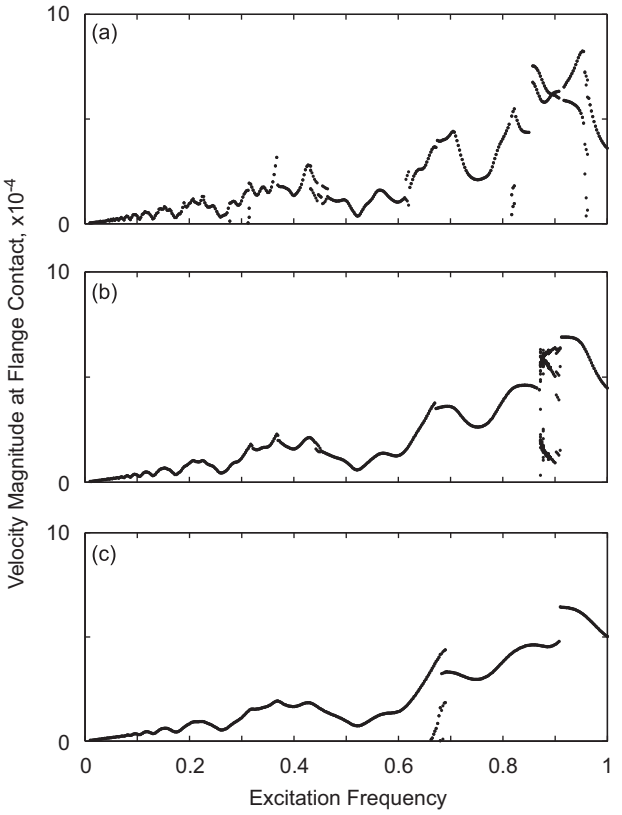

Fig. 4. Magnitude of the string's frequency response as a function of modal damping for (a) $\zeta = 0.02$, (b) $\zeta = 0.04$, and (c) $\zeta = 0.06$.

parameters in Table 1 is symmetric (the magnitudes of the impacts against the upper and lower flanges are equal) at most frequencies, with exceptions near $\omega = 0.37$, 0.45, and 0.67 as shown in Fig. 2(b). Multiple points at a given frequency in the response are indicative of the string impacting and rebounding from a flange multiple times per period of the excitation, and a single point indicates that one impact per flange occurred per period of the excitation with an equal velocity at the upper flange as at the lower flange. The response is described using a $Y - Z_L - Z_U$ convention, in which the response exhibits period Y motion with Z_L impacts per period of the excitation cycle on the lower flange and Z_U impacts on the upper flange. For symmetric responses $Z_L = Z_U = Z$, the magnitudes of the velocity of the string at contact with the upper and lower flanges are equal, and the response is concisely described with the notation $Y - Z$. For example, for the case shown in Fig. 2(b), asymmetric 1–1–1 motion is observed (in which the magnitude of the velocity at impact against the upper flange is different than against the lower flange) at $\omega = 0.445$ (Fig. 3(a)) with one impact for the upper flange and one impact for the lower flange per period of the excitation repeating every period of the excitation, symmetric 1–1 motion with one impact per flange per period of the excitation at $\omega = 0.87245$ (Fig. 3(b)), 1–3 motion at $\omega = 0.87248$ (Fig. 3(c)), 3–2 motion at $\omega = 0.9240$ (Fig. 3(d)), and 1–2 motion at $\omega = 0.94$ (Fig. 3(e)). Contact with the flanges in each of these cases occurs at $w = \pm 1.9 \times 10^{-4}$, as indicated by the sudden change in velocity in the phase projections.

The convergence of the frequency response is shown in Fig. 2 as the number of modes N is increased from 5 (Fig. 2(a)) to 100 (Fig. 2(c)). The response of the string does not significantly change for $N > 10$ (Fig. 2(b)). Unlike stationary strings or beams, the traveling string of Fig. 1(a) cannot be accurately approximated up to the first natural frequency by only three to five modes [28,29], as an unstable response is incorrectly predicted near $\omega = 0.68$ for $N = 5$. In Fig. 4, the modal damping is varied from $\zeta = 0.02$ (Fig. 4(a)) to 0.06 (Fig. 4(c)). As the modal damping is increased, the system's response becomes more symmetric, such that there is only one narrow window of asymmetric motion near $\omega = 0.68$ for $\zeta = 0.6$ (Fig. 4(c)), though the discontinuity in the frequency response persists near $\omega \approx 0.925$.

One method of classifying the stability of a nonlinear system is through the use of Lyapunov exponents, which measure the rate of divergence/convergence of a system at a given state. Positive Lyapunov exponents indicate an aperiodic or chaotic state while negative exponents are found in convergent states that exhibit periodic, steady-state behavior. Lyapunov exponents are calculated based on the system's Jacobian; however, for continuous systems with nonlinear constraints that render the Jacobian to be state dependent, this method is unable to be applied [30]. Alternative methods exist for calculating the Lyapunov exponents in systems with impacts that require the coupling of multiple similar systems [31] or coefficient of restitution models [32]. In what follows, the finite-time Lyapunov exponent method of [33] is applied.

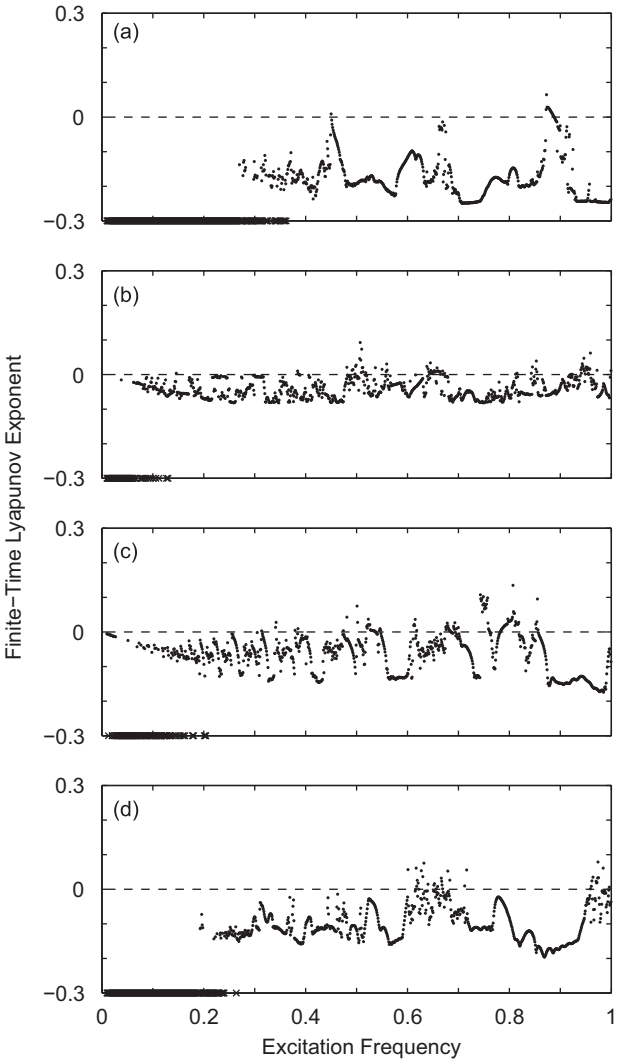

Fig. 5. Finite-time Lyapunov exponents for (a) the baseline case, (b) $v = 0.816$, (c) $d_{-1} = d_1 = 3.87 \times 10^{-4}$, and (d) $\ell_1 = 0.75$; in each case, only the parameter indicated differs from the values list in Table 1.

This method involves the calculation of a Jacobian-like quantity based on the response of the system over a finite time period with initial conditions that are varied for each modal coordinate by an amount several orders of magnitude below the steady-state modal amplitudes. In all cases, the finite-time Lyapunov exponents are found to converge for a simulation time of 50 periods of the excitation. For the baseline case (the system with parameters described by Table 1), the finite-time Lyapunov exponents are shown as a function of excitation frequency in Fig. 5(a). For $\omega = 0.45$ (where the system transitions from symmetric 1–1 motion to asymmetric 1–1–1 motion) and $\omega \in (0.87, 0.89)$ (where the system exhibits a chaotic response), the finite-time Lyapunov exponents are found to be positive. Points on the graph that appear as x's along the abscissa indicate that the finite-time Lyapunov exponent for that frequency tends towards $-\infty$.

As the transport speed of the system is increased from $v = 0.068$ (Fig. 6(a)) to 0.816 (Fig. 6(d)), the response becomes more asymmetric, as indicated by the multiple stable branches in the frequency response. For a low transport speed (Fig. 6(a)), the response of the system is predominantly 1–1 motion. Increasing v by a factor of four (Fig. 6(b)) increases the number of bifurcations and results in the asymmetric responses extending over a broader range of frequencies. At higher transport speeds (Fig. 6(c), (d)), the system exhibits 2–1–1 and higher motion, including a potentially chaotic response near $\omega = 0.79$, with windows of 1–1 motion (such as near $\omega = 0.62$) shown in Fig. 6(d). Thus, for $v \geq 0.272$, a critical bifurcation threshold is exceeded [1], increases above which result in the system becoming less stable and exhibiting higher periodic and aperiodic motion. The finite-time Lyapunov exponent for $v = 0.816$ is shown in Fig. 5(b). Regions of positive finite-time Lyapunov exponents are particularly prominent adjacent to the windows of 1–1 motion (for instance, for $\omega \leq 0.56$ and $\omega \geq 0.64$).

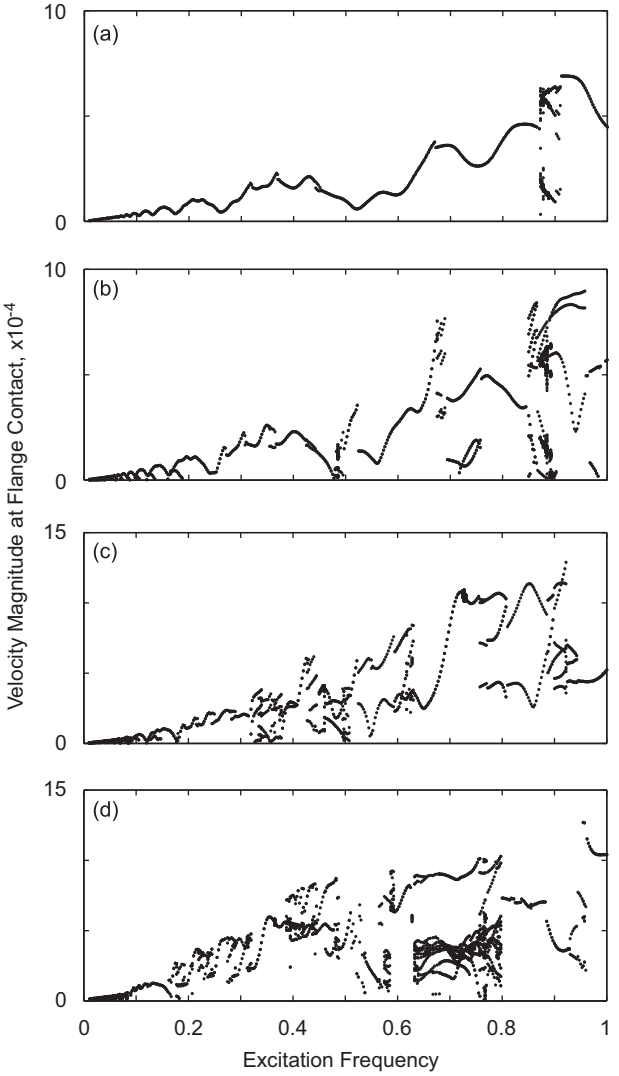

Fig. 6. Magnitude of the string's frequency response as a function of transport speed (a) $v = 0.068$, (b) $v = 0.272$, (c) $v = 0.544$, and (d) $v = 0.816$.

The nonlinear guides are described by five parameters: clearance, stiffness, symmetry in terms of the flange stiffness and offset, and position. Two cases of flange clearance are considered: positive clearances and negative clearances, which result in preloads. Similar to other systems with piecewise-linear constraints [34], the system's response is dominated by the nonlinearity of the guide. Several types of critical thresholds exist as the system transitions from the case where the clearance of the flanges exceeds the displacement of the string at $x = \ell_1$ ($d_{-1} = d_1 > 4 \times 10^{-4}$) to a nonlinear guide ($0 < d_{-1} = d_1 \leq 4 \times 10^{-4}$) to a linear spring ($d_{-1} = d_1 = 0$). The higher critical threshold occurs for the clearance where the string just grazes the flanges. At $d_{-1} = d_1 = 3.8 \times 10^{-4}$ (Fig. 7(a)), the string grazes the flanges at low frequencies, indicated by the approximately zero velocity magnitude for $\omega \leq 0.2$, and grazing bifurcations occur as the frequency is increased, signified by the sudden jumps in the frequency response. As this threshold is approached from below, the width of any stable bands in the response decreases and eventually becomes unstable, and the system exhibits asymmetric responses with narrow windows of 1–1 motion, behavior that is also observed in stationary strings with a compliant amplitude constraint [35]. The lower critical threshold is an asymmetric response threshold that occurs as the clearance is increased from the linear spring case (Fig. 8(d)) to one-tenth of the baseline clearance (Fig. 8(c)). Near $\omega = 0.85$, the system's response is 1–1–1 motion. Further increases of the clearance reduces the frequency range of the asymmetric response (Fig. 8(b)), and the response transitions from windows of asymmetric motion to windows of period doubling (Fig. 8(a)). Increases in the clearance to the baseline clearance and above (Fig. 7(d)) results in windows in which the periodicity of the system increases such that 4–1 and higher symmetric responses are observed. At twice the baseline clearance(Fig. 7(a)), chaotic motion is observed over multiple ranges as is evident in the positive finite-time Lyapunov exponents (Fig. 5(c)) near

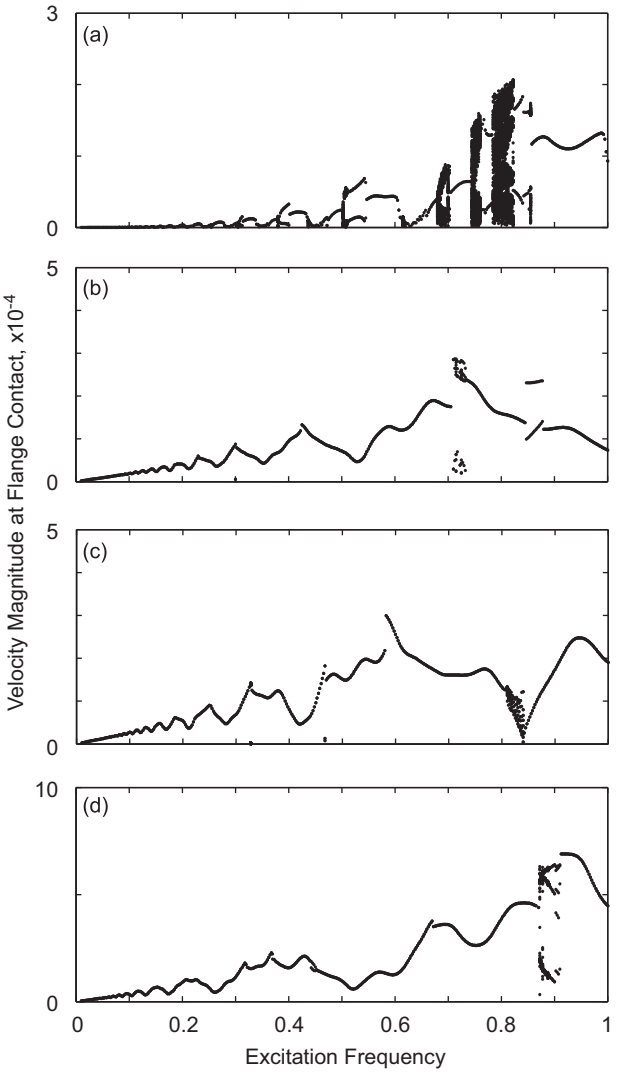

Fig. 7. Magnitude of the string's frequency response as a function of the guide's clearance for (a) $d_{-1} = d_1 = 3.87 \times 10^{-4}$, (b) $d_{-1} = d_1 = 3.38 \times 10^{-4}$, (c) $d_{-1} = d_1 = 2.85 \times 10^{-4}$, and (d) $d_{-1} = d_1 = 1.93 \times 10^{-4}$.

$\omega = 0.345$, 0.5, 0.615, 0.69, 0.75, 0.8, and 0.85. Above $\omega = 0.85$, the finite-time Lyapunov exponents remain below zero for the remainder of the frequencies studied, which corresponds to the symmetric 1–1 motion observed in (Fig. 7(a)).

As the clearance is decreased to zero (Fig. 8(d)), the system becomes linear, and the string exhibits only 1–1 motion over the frequency range investigated. The first natural frequency of the string when it is in constant contact with the guide is $\omega = 5.55$ due to the added stiffness to the system, significantly above the frequency range shown here. As the clearance is further reduced to a negative value, the guide becomes preloaded. Preloads can cause instabilities in certain regions of the parameter space, and as the preload is increased, the frequency range of any stable, period one response decreases and eventually becomes unstable [36,37]; however, in this string model, the bending stiffness of the web is neglected and the string is unable to displace against the preloaded flange. Consequently, the preload does not cause unstable behavior in the frequency range studied. As the preload is increased from 0 to 1.43×10^{-3} ($y_{-1} = -y_1 = 4.83 \times 10^{-5}$, the magnitude of which is equivalent to 25 percent of the baseline clearance), the velocity magnitude at flange contact decreases to zero and the response of the string is 1–1 motion. For preloads greater than 1.43×10^{-3}, the string is unable to displace the flange for $0 < \omega \leq 1$, and the guide effectively becomes a pinned boundary.

The effect of the stiffness of the flanges on the frequency response is reported in Fig. 9. For a low flange stiffness $k_{-1} = k_1 = 0.3$ (Fig. 9(a)), the system exhibits a 1–1 response for $0 < \omega \leq 1$. Increasing the stiffness to $k_{-1} = k_1 = 3$ (Fig. 9(b)) yields an asymmetric response with a periodicity greater than one near $\omega = 0.73$. However, further increases of the stiffness above the baseline case (Fig. 9(c)) decreases the range of frequencies over which the asymmetric response is observed until the asymmetric response vanishes (Fig. 9(e)). The multiple branches of the solution observed for $k_{-1} = k_1 = 3000$ (Fig. 9(e)) near $\omega = 0.35$, 0.40, 0.58, and 0.76 are 2–1 motion. Unlike the critical bifurcation thresholds associated

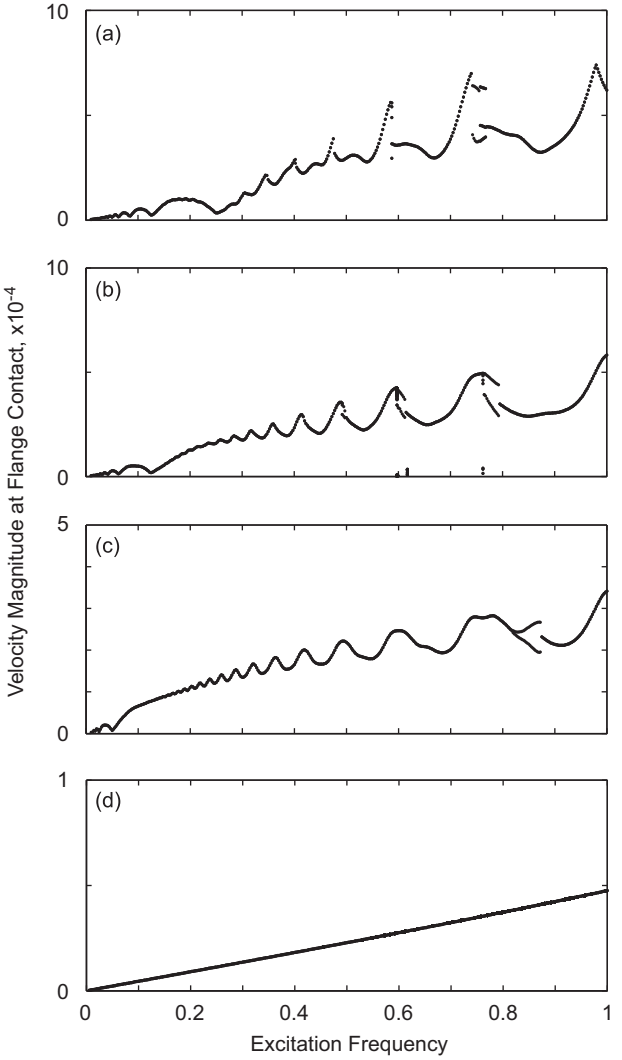

Fig. 8. Magnitude of the string's frequency response as a function of the guide's clearance for (a) $d_{-1} = d_1 = 9.67 \times 10^{-5}$, (b) $d_{-1} = d_1 = 4.83 \times 10^{-5}$, (c) $d_{-1} = d_1 = 1.93 \times 10^{-5}$, and (d) $d_{-1} = d_1 = 0$.

with the clearance of the flanges, the system's response does not exhibit more complicated behavior than 2–1 motion as the stiffness is increased. Increasing the stiffness above $k_{-1} = k_1 = 3000$ does not result in any appreciable change in the frequency response, indicating that this is effectively a rigid flange that the string does not compress.

The symmetry of the system is characterized both by the force–deflection profile of the guide and by the position of the guide along the length of the string. The effect of the asymmetry of the stiffness of the flanges on the frequency response is shown in Fig. 10. In the limiting case of $k_{-1} = 0$ (Fig. 10(a)), the system reduces to a one-sided constraint that strictly exhibits 1–1 motion away from $\omega = 0.65$. Increasing the stiffness of the lower flange to $k_{-1} = 3$ (Fig. 10(b)) yields 1–1–1 motion. For $k_{-1} > k_1$, the number of bifurcations increases as well as the range of frequencies they are stable over, eventually resulting in 4–1–1 and higher asymmetric motions (Fig. 10(d)). Values of $k_{-1} \geq 3000$ (Fig. 10(e)) produce no discernable changes in the frequency response as the string no longer appreciably displaces the lower flange.

The symmetry of the flange's location, or offset of the flanges, while the distance between the flanges is held constant is varied from the symmetric case (Fig. 11(e)) to the center of the guide being located 1.93×10^{-4} from the string's neutral axis (Fig. 11(a)). At low frequencies, the string grazes against the upper flange when the flanges are offset 1.93×10^{-4} from the string's neutral axis, and near $\omega = 0.62$ the upper flange is not engaged. The motion for this case is predominantly 1–1–1 motion, with windows of 1–2–1 motion and 1–1–0 motion. As the offset is reduced, the frequency range increases over which the number of impacts per period of the excitation is different for the two flanges, and the number of impacts

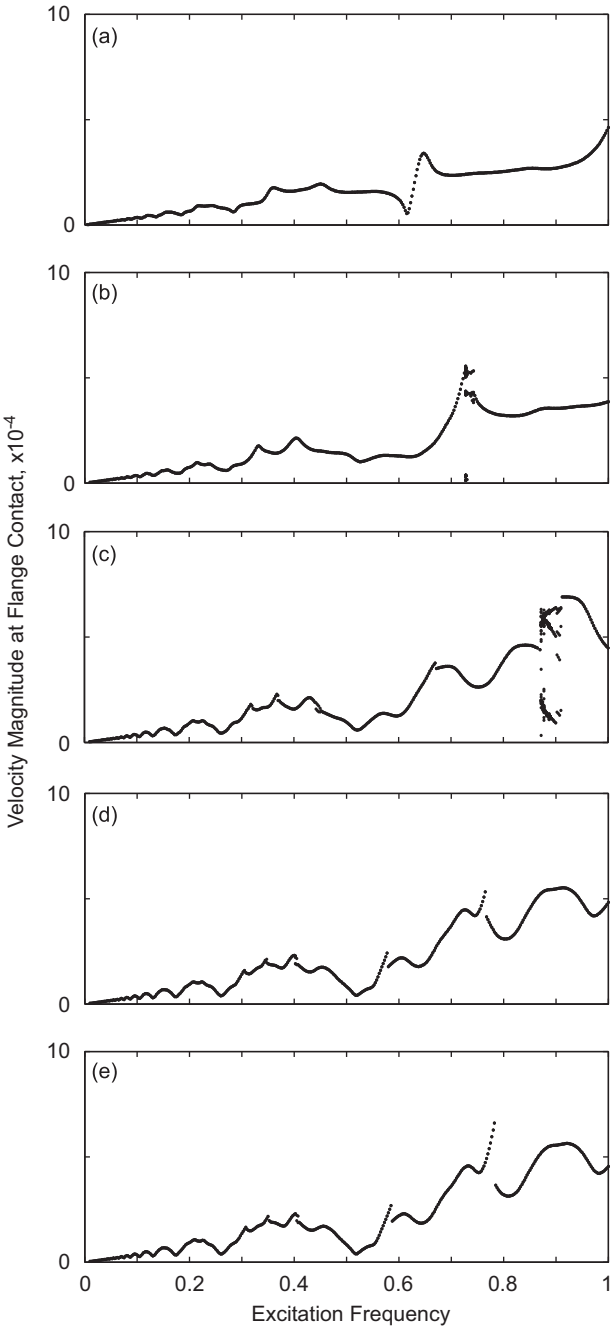

Fig. 9. Magnitude of the string's frequency response as a function of the guide's stiffness for (a) $k_{-1} = k_1 = 0.3$, (b) $k_{-1} = k_1 = 3$, (c) $k_{-1} = k_1 = 30$, (d) $k_{-1} = k_1 = 300$, and (e) $k_{-1} = k_1 = 3000$.

per period increases as well. For the offset of 9.67×10^{-5} (Fig. 11(c)), 1–2–4 motion is observed. As the offset is further reduced to 4.83×10^{-5} (Fig. 11(d)), the periodicity increases such that 4–2–4 motion is observed.

The position of the nonlinear guide along the string is varied in Fig. 12. When the guide is located near the excitation (Fig. 12(a)), the response of the string is 1–1 motion except near $\omega = 0.77$. As the guide is moved towards the pinned boundary, the magnitude of the velocity at flange contact decreases and the frequency range that the asymmetric responses are stable over increases, particularly for $\ell_1 \geq 0.625$ (Fig. 12(d)). For $\ell_1 = 0.75$, the string grazes the flanges at low frequencies, similar to the case of $d_{-1} = d_1 = 3.8 \times 10^{-4}$ (Fig. 7(a)), and chaotic regions occur in the frequency response for $0.6 < \omega < 0.7$ and for $\omega > 0.96$, as is indicated by the positive finite-time Lyapunov exponents in Fig. 5(d).

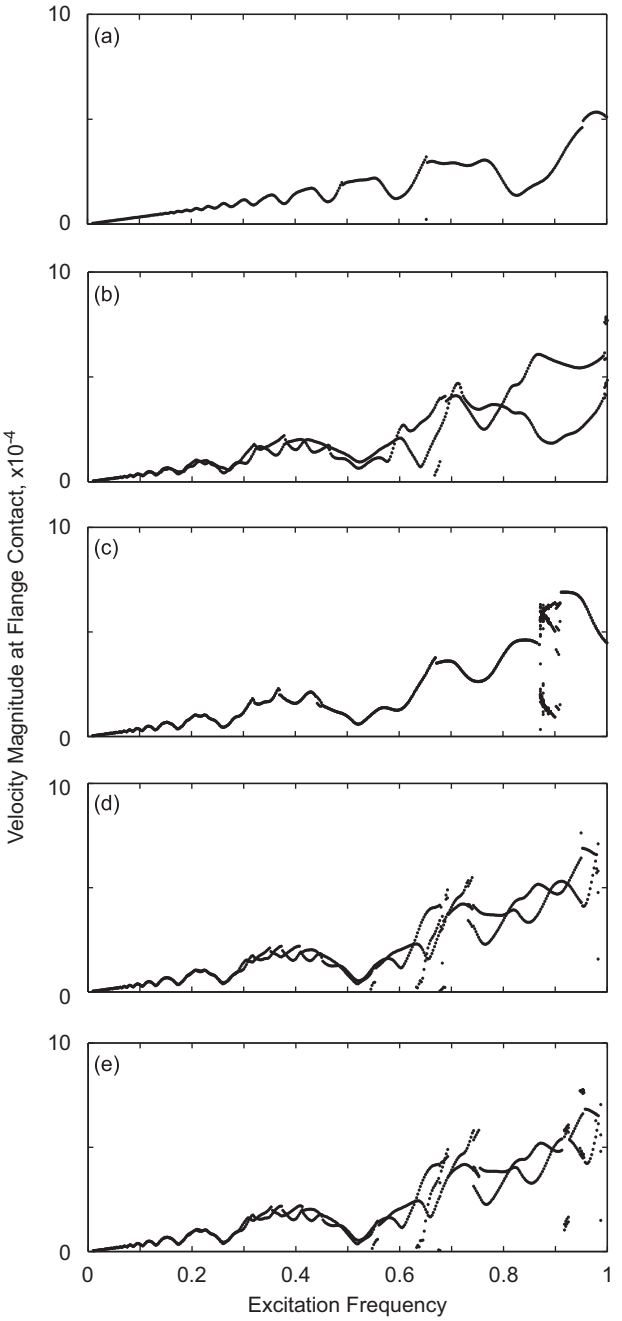

Fig. 10. Magnitude of the string's frequency response as a function of the asymmetry of the guide's flange stiffnesses for (a) $k_{-1}=0$, (b) $k_{-1}=3$, (c) $k_{-1}=30$, (d) $k_{-1}=300$, and (e) $k_{-1}=3000$; $k_1=30$.

4. Summary

A method for performing modal analysis on gyroscopic systems with nonlinear constraints is developed. This method assumes that the nonlinear constraint can be expressed as a piecewise linear force–deflection profile located at an arbitrary position within the domain. The system is divided into two contiguous regions at the point of the nonlinear constraint, and a superposition function is chosen such that homogeneous boundary conditions result. With the piecewise linear assumption for the constraint, the mode shapes and natural frequencies are calculated in each state. A mapping method based on the inner products of the mode shapes is developed to map the displacement of the system between the in-contact and out-of-contact states. This method is illustrated with a model for the vibration of a traveling string in contact with a piecewise-linear constraint as an analog of the interaction between magnetic tape and a guide in data storage

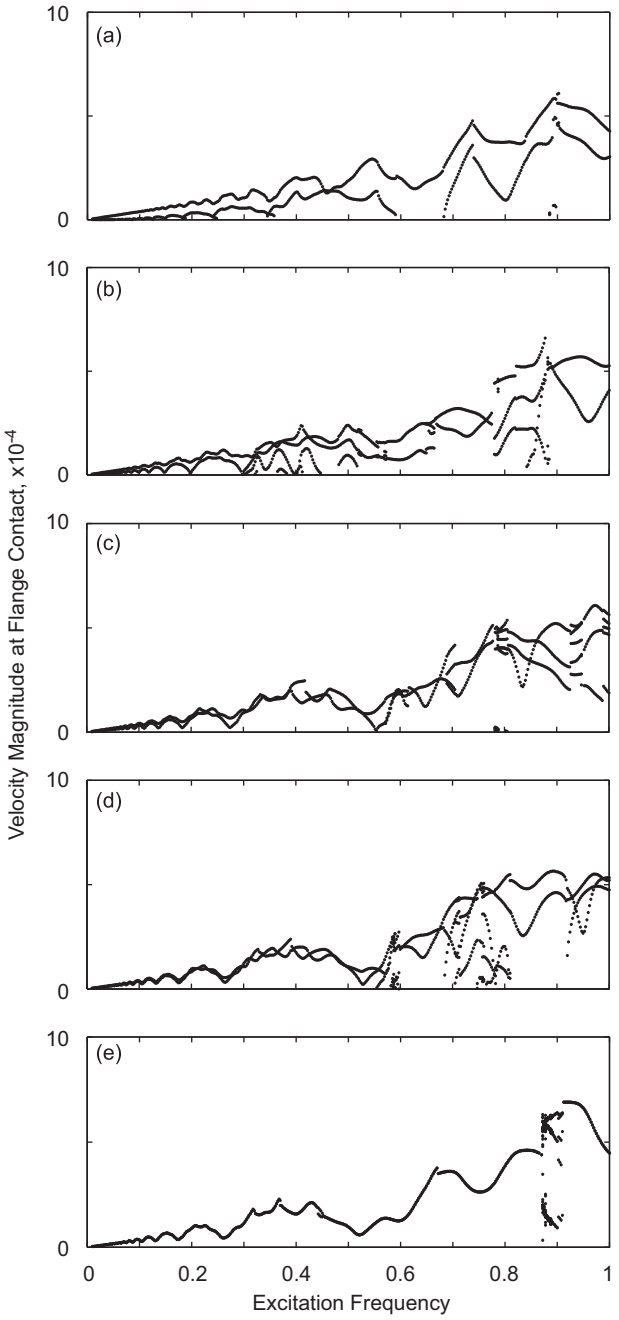

Fig. 11. Magnitude of the string's frequency response as a function of the flange offset from the string's neutral axis for (a) $d_{-1}=0$ and $d_1=3.87\times10^{-4}$, (b) $d_{-1}=4.83\times10^{-5}$ and $d_1=3.38\times10^{-4}$, (c) $d_{-1}=9.67\times10^{-5}$ and $d_1=2.85\times10^{-4}$, (d) $d_{-1}=1.45\times10^{-4}$ and $d_1=2.42\times10^{-4}$, and (e) $d_{-1}=d_1=1.93\times10^{-4}$.

systems. Five design parameters of the nonlinear constraint are considered in parameter studies: flange clearance, flange stiffness, symmetry of the force–deflection profile in terms of stiffness and offset, and the guide's position along the length of the string. There are critical bifurcation thresholds, below which the system exhibits period one, symmetric behavior, and above which the system contains asymmetric, higher periodic motion with windows of chaotic behavior. These bifurcation thresholds are particularly pronounced for the transport speed, flange clearance, symmetry of the force deflection profile, and guide position.

The results of this study are particularly useful for the tape drive industry. For the goals of the industry roadmap [38], in which the tape transport speed is expected to significantly increase, new guide and path designs are needed to mitigate the higher periodicity dynamics introduced by increasing the transport speed. Using the conclusions drawn from varying

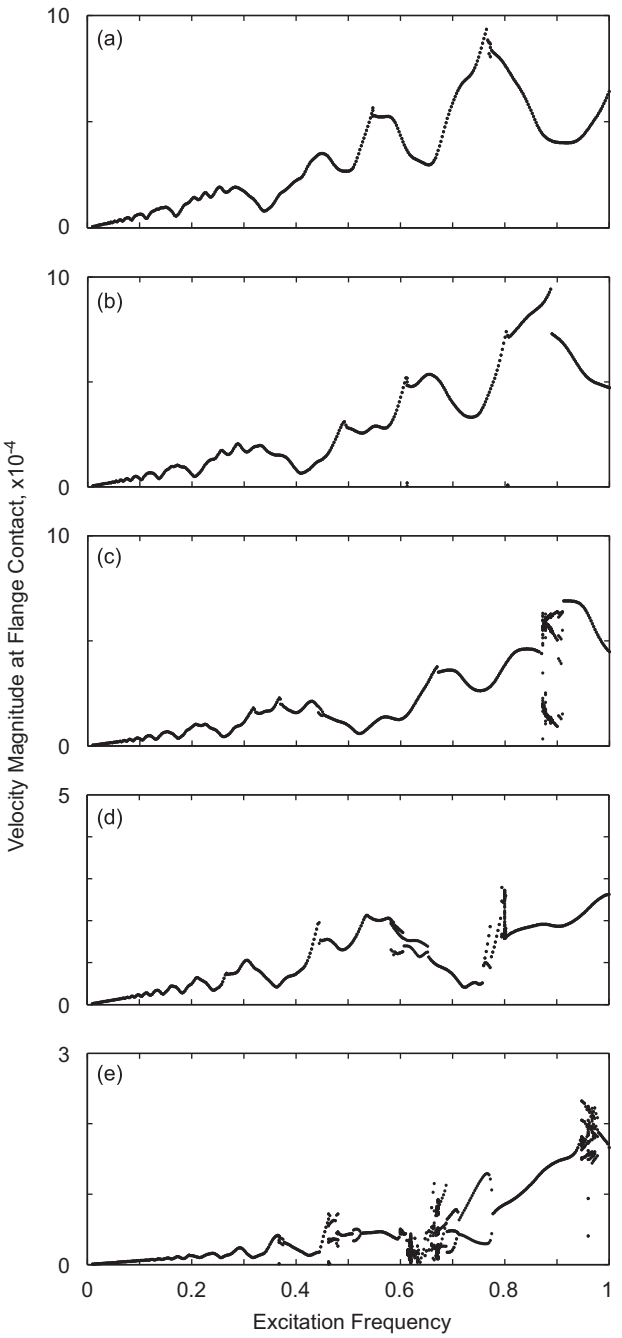

Fig. 12. Magnitude of the string's frequency response as a function of the guide's position for (a) $\ell_1 = 0.25$, (b) $\ell_1 = 0.375$, (c) $\ell_1 = 0.5$, (d) $\ell_1 = 0.625$, and (e) $\ell_1 = 0.75$.

flange stiffnesses and symmetry, as well as the position of the guides with respect to disturbance sources, is one method to better condition the lateral tape dynamics.

The primary contributions and conclusions of this investigation are:

1. The stability of the system is sensitive to the system's velocity, and, compared to stationary systems, more mode shapes are needed to accurately model the dynamics of the system.
2. When the flange stiffness is symmetric, the system exhibits period one symmetric behavior over most frequency ranges; however, for asymmetric stiffness profiles the system's stability decreases as one flange is increased in stiffness compared to the other.

3. Both asymmetric and period doubling bifurcation thresholds exist in the parameter space for the flange clearance. As the clearance is reduced, period one asymmetric behavior dominates the response, and as the clearance is increased, higher periodic symmetric behavior is predominant.
4. For systems with asymmetric flange clearances, the stability of the system is improved by increasing the asymmetry of the clearances.
5. Varying the position of the nonlinear constraint along the domain results in behavior that is similar to varying the clearance of the constraint. Moving the constraint closer to the excitation source results in symmetric period one behavior, and moving it away from the excitation source results in higher periodic behavior and grazing bifurcations.

Acknowledgments

The authors gratefully acknowledge the support from the Information Storage Industry Consortium. The authors would also like to thank Carnegie Mellon University's Department of Mechanical Engineering, where this research was conducted, and Prof. Bill Messner for his feedback on drafts of this paper.

References

[1] L. Zuo, A. Curnier, Non-linear real and complex modes of conewise linear systems, *Journal of Sound and Vibration* 174 (1994) 289–313.
[2] M.P. Païdoussis, C. Semler, Nonlinear and chaotic oscillations of a constrained cantilevered pipe conveying fluid: a full nonlinear analysis, *Nonlinear Dynamics* 4 (1993) 655–670.
[3] W.D. Zhu, C.D. Mote Jr., Propagation of boundary disturbances in an axially moving strip in contact with rigid and flexible constraints, *ASME Journal of Applied Mechanics* 62 (1995) 873–879.
[4] W.T. van Horssen, S.V. Ponomareva, On the construction of an equation describing an axially moving string, *Journal of Sound and Vibration* 287 (2005) 359–366.
[5] J.A. Wickert, C.D. Mote Jr., Classical vibration analysis of axially moving continua, *ASME Journal of Applied Mechanics* 57 (1990) 738–744.
[6] N.C. Perkins, Linear dynamics of a translating string on an elastic foundation, *ASME Journal of Vibration and Acoustics* 112 (1990) 2–7.
[7] S.-P. Cheng, N.C. Perkins, The vibration and stability of a friction-guided, translating string, *Journal of Sound and Vibration* 144 (1991) 281–292.
[8] G. Chakraborty, A.K. Mallik, Non-linear vibration of a travelling beam having an intermediate guide, *Nonlinear Dynamics* 20 (1999) 247–265.
[9] D. Jiang, C. Pierre, S.W. Shaw, Large-amplitude non-linear normal modes of piecewise linear systems, *Journal of Sound and Vibration* 272 (2004) 869–891.
[10] A.C.J. Luo, The mapping dynamics of periodic motions for a three-piecewise linear system under a periodic excitation, *Journal of Sound and Vibration* 283 (2005) 723–748.
[11] G. Kerschen, K. Worden, A.F. Vakakis, J.-C. Golinval, Past, present and future of nonlinear system identification in structural dynamics, *Mechanical Systems and Signal Processing* 20 (2006) 505–592.
[12] E.K. Ervin, J.A. Wickert, Repetitive impact response of a beam structure subjected to harmonic base excitation, *Journal of Sound and Vibration* 307 (2007) 2–19.
[13] P. Metallidis, S. Natsiavas, Vibration of a continuous system with clearance and motion constraints, *International Journal of Non-Linear Mechanics* 35 (2000) 675–690.
[14] S. Deshpande, S. Mehta, G.N. Jazar, Optimization of secondary suspension of piecewise linear vibration isolation systems, *International Journal of Mechanical Sciences* 48 (2006) 341–377.
[15] G.W. Luo, Dynamics of an impact-forming machine, *International Journal of Mechanical Sciences* 48 (2006) 1295–1313.
[16] M.H. Fredriksson, D. Borglund, A.B. Nordmark, Experiments on the onset of impacting motion using a pipe conveying fluid, *Nonlinear Dynamics* 19 (1999) 261–271.
[17] N. Qiao, W. Lin, Q. Qin, Bifurcations and chaotic motions of a curved pipe conveying fluid with nonlinear constraints, *Computers and Structures* 84 (2006) 708–717.
[18] W. Lin, N. Qiao, H. Yuying, Dynamical behaviors of a fluid-conveying curved pipe subjected to motion constraints and harmonic excitations, *Journal of Sound and Vibration* 306 (2007) 955–967.
[19] J.A. Wickert, C.D. Mote Jr., Current research on the vibration and stability of axially-moving materials, *Shock and Vibration Digest* 20 (1988) 3–13.
[20] G.E. Young, K.N. Reid, Lateral and longitudinal dynamic behavior and control of moving webs, *ASME Journal of Dynamic Systems, Measurement, and Control* 115 (1993) 309–317.
[21] J.B. Yerashunas, J.A.D. Abreu-Garcia, T.T. Hartley, Control of lateral motion in moving webs, *IEEE Transactions on Control Systems Technology* 11 (2003) 684–693.
[22] L.-Q. Chen, Analysis and control of transverse vibrations of axially moving strings, *ASME Applied Mechanics Reviews* 58 (2005) 91–116.
[23] M.R. Brake, J.A. Wickert, Frictional vibration transmission from a laterally moving surface to a traveling beam, *Journal of Sound and Vibration* 310 (2008) 663–675.
[24] L. Meirovitch, I.G. Ryland, Response of slightly damped gyroscopic systems, *Journal of Sound and Vibration* 67 (1979) 1–19.
[25] V. Kartik, J.A. Wickert, Vibration and guiding of moving media with edge weave imperfections, *Journal of Sound and Vibration* 291 (2006) 419–436.
[26] L. Azrar, E.H. Boutyour, M. Potier-Ferry, Non-linear forced vibrations of plates by an asymptotic-numerical method, *Journal of Sound and Vibration* 252 (2002) 657–674.
[27] C.J. Begley, L.N. Virgin, Impact response and the influence of friction, *Journal of Sound and Vibration* 211 (1998) 801–818.
[28] D.J. Wagg, S.R. Bishop, Application of non-smooth modeling techniques to the dynamics of a flexible impacting beam, *Journal of Sound and Vibration* 256 (2002) 803–820.
[29] K.J.L. Fegelman, K. Grosh, Dynamics of a flexible beam contacting a linear spring at low frequency excitation: experiment and analysis, *ASME Journal of Vibration and Acoustics* 124 (2004) 237–249.
[30] M.P. Païdoussis, G.X. Li, Cross-flow-induced chaotic vibrations of heat-exchanger tubes impacting on loose supports, *Journal of Sound and Vibration* 152 (1992) 305–326.
[31] A. Stefanski, Estimation of the largest Lyapunov exponent in systems with impacts, *Chaos, Solitons and Fractals* 11 (2000) 2443–2451.
[32] S.L.T. de Souza, I.L. Caldas, Calculation of Lyapunov exponents in systems with impacts, *Chaos, Solitons and Fractals* 19 (2004) 569–579.
[33] S.C. Shadden, F. Lekien, J.E. Marsden, Definition and properties of Lagrangian coherent structures from finite-time Lyapunov exponents in two-dimensional aperiodic flows, *Physica D* 212 (2005) 271–304.
[34] E.L.B. van de Vorst, D.H. van Campen, A. de Kraker, Periodic solutions of a multi-dof beam system with impact, *Journal of Sound and Vibration* 192 (1996) 913–925.

[35] K.D. Murphy, T.M. Morrison, Grazing instabilities and post-bifurcation behavior in an impacting string, *Journal of the Acoustical Society of America* 111 (2002) 884–892.
[36] H.Y. Hu, Primary resonance of a harmonically forced oscillator with a pair of symmetric set-up elastic stops, *Journal of Sound and Vibration* 207 (1997) 393–401.
[37] A. Maccari, The response of a forced oscillator under the effect of a pair of set-up elastic stops, *Journal of Sound and Vibration* 235 (2000) 879–887.
[38] D. Mee (Ed.), *International Magnetic Tape Storage Roadmap*, *Information Storage Industry Consortium*, 2005.